Accepted Manuscript

Development of a novel cell structure for low-temperature SOFC using porous stainless steel support combined with hydrogen permeable Pd layer and thin film proton conductor

Tetsuro Kariya, Hiroki Tanaka, Tomoki Hirono, Tetsuji Kuse, Katsu Yanagimoto, Kiyoshi Uchiyama, Mitsunori Henmi, Mitsutaka Hirose, Isao Kimura, Koukou Suu, Hiroshi Funakubo

PII: S0925-8388(15)31085-9

DOI: 10.1016/j.jallcom.2015.09.109

Reference: JALCOM 35384

To appear in: *Journal of Alloys and Compounds*

Received Date: 17 June 2015

Revised Date: 3 September 2015

Accepted Date: 13 September 2015

Please cite this article as: T. Kariya, H. Tanaka, T. Hirono, T. Kuse, K. Yanagimoto, K. Uchiyama, M. Henmi, M. Hirose, I. Kimura, K. Suu, H. Funakubo, Development of a novel cell structure for low-temperature SOFC using porous stainless steel support combined with hydrogen permeable Pd layer and thin film proton conductor, *Journal of Alloys and Compounds* (2015), doi: 10.1016/j.jallcom.2015.09.109.

Proposed novel cell structure for low-temperature SOFC

<Proposed novel cell structure>

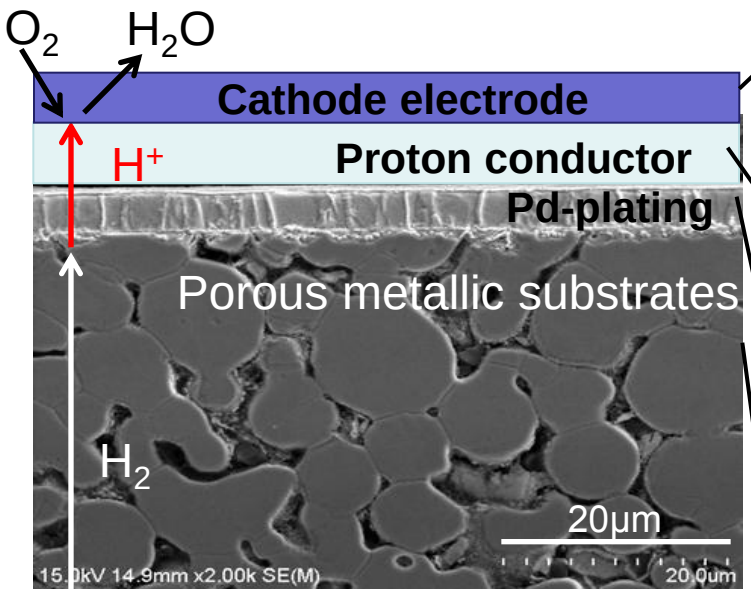

<Cell performance>
Cell performance at low temperature of 400° C was demonstrated for the first time.

Thin cathode layer $(La_{0.6}Sr_{0.4})(Co_{0.2}Fe_{0.8})O_{3-\delta}$
- good oxygen ion conductor
- good electric conductivity
- thin film, 100nm thick

Thin proton conductor $Sr(Zr_{0.8}Y_{0.2})O_{3-\delta}$
- proton conductive at low temperature (400° C)
- thin film, 1.2 μm (higher conductivity)
- good insulating property
- lattice parameter and thermal expansion coefficient are close to Pd

Dense and thin hydrogen permeable layer Pd-plating
- good proton conductivity and electric conductivity
- good for the deposition of thin proton conductor on it
- separating H_2 and O_2
- replaced by other cost effective hydrogen permeable materials like Nb,V, and those alloys

Porous metallic substrates (sintered Fe-17Cr ferritic alloy powders)
- strong mechanical properties (toughness, thermal shock resistance)
- superior electric conductivity
- thermal expansion coefficient (11.9) is close to Pd (11.8) and $Sr(Zr_{0.8}Y_{0.2})O_{3-\delta}$ (9.87) $x10^{-6}/K$

Development of a novel cell structure for low-temperature SOFC using porous stainless steel support combined with hydrogen permeable Pd layer and thin film proton conductor

*Tetsuro Kariya [1, 2)], Hiroki Tanaka [1)], Tomoki Hirono [2)], Tetsuji Kuse [2)], Katsu Yanagimoto[2)], Kiyoshi Uchiyama [3)], Mitsunori Henmi [4)], Mitsutaka Hirose [4)], Isao Kimura [4)], Koukou Suu [4)], and Hiroshi Funakubo [1)]

[1)] Department of Innovative and Engineered Materials, Tokyo Institute of Technology, Yokohama 226-8502, Japan

[2)] Sanyo Special Steel Co., Ltd, Himeji, Hyogo 672-8677, Japan

[3)] Tsuruoka National College of Technology, Tsuruoka, Yamagata 997-8511, Japan

[4)] ULVAC, Inc., Chigasaki, Kanagawa 253-8543, Japan

*Corresponding author. 3007, Nakashima, Shikama-ku, Himeji-shi 672-8677, Japan Tel. +81 79 235 6143, Fax. +81 79 235 6157, E-mail address: tkariya@himeji.sanyo-steel.co.jp

Abstract

A novel cell structure for low-temperature SOFC was proposed, using porous stainless steel support substrates combined with thin hydrogen permeable Pd layers, thin-film proton conductor, and thin-film cathode. Metallic supports consist of sintered ferritic stainless steel spherical powders whose thermal expansion coefficient is close to that of the hydrogen permeable layers and proton conductive electrolytes. To prepare the cell, both the 1.2-μm thick proton conductive $Sr(Zr_{0.8}Y_{0.2})O_{3-\delta}$ electrolyte layer and the 100-nm thick $(La_{0.6}Sr_{0.4})(Co_{0.2}Fe_{0.8})O_{3-\delta}$ cathode layer were deposited by pulsed laser deposition (PLD) on a Pd-coated porous ferritic stainless steel substrate. The power generation performance at a low temperature of 400 °C was demonstrated in this proposed cell for the first time, while obtained power density is still low and improvements are required.

Keywords: Solid oxide fuel cell, Proton conductor, Metal powder, Porous substrate, low temperature

1. Introduction

Solid oxide fuel cells (SOFC) are promising energy conversion devices. In addition to superior power generation efficiency, there is no necessity to use high-purity gas, which makes it possible for the SOFC to use current fuel distribution infrastructure [1-2]. The major issues for the SOFC are its high operating temperature ranging from 700 to 1000 °C and low reliability due to the use of ceramic support with fragile mechanical properties in view of its mechanical strength and thermal shock resistance [3-4]. In fact, various shapes of SOFC such as tubular and planar designs have been investigated in terms of lower production cost, higher power density per unit volume, and superior reliability [2-3]. Therefore, enhancing mechanical reliability of the cell is one of the important challenges.

In order to overcome these issues, using metallic supports is ideal, which generally show improved mechanical properties and structural reliability compared with ceramic materials. Furthermore, the metallic support could contribute to lower internal electrical cell resistance compared to ceramic supports due to higher electric conductivity, which can extend cell performance. To realize metal supports, reducing the operating temperature of SOFC to below 600 °C, and preferably below 400 °C, is important for inhibiting the oxidization of the metallic components. However, low-temperature SOFC using metallic support has hardly been investigated.

In this study, we propose a novel cell structure that employs a porous stainless steel support substrate combined with a thin film proton conductive electrolyte for low-temperature SOFC. Proton conductors with the perovskite structure show higher ionic conductivities compared with conventional oxygen ion conductors such as ZrO_2 stabilized by Y_2O_3 (YSZ) at lower temperatures [5-9]. Another important key factor for the proton conductive electrolyte layer for low-temperature SOFC is to reduce its thickness as thin as possible because ionic mobility, significant for more reduced ohmic losses, is generally reduced at lower temperatures. In addition, proton conductivities

of major candidates are usually still low [10-11].

2. Proposal of the novel cell structure for low-temperature SOFC

2.1. Proposed stack structure of the cell

Figure 1 illustrates our proposed novel cell structure using a porous stainless steel support substrate. In this structure, the stainless steel support substrate has to be porous to supply and transfer hydrogen gas for power generation. Spherical powders produced by nitrogen gas atomization were selected for preparing the sintered porous substrate because evenly dispersed pores are obtained by using spherical powders and those pores are important for uniform and stable supply of hydrogen gas.

Depositing a dense thin-film of proton conductor directly on a porous substrate is difficult, therefore, coating by a hydrogen permeable-layer is employed on the sintered porous stainless steel support to fill the pores in the surface before depositions of the thin-films of the electrolyte and cathode layers. As a consequence, it is possible to deposit dense thin films of the proton conductive electrolyte. Although, Pd-plating was used as hydrogen permeable material [12] in this study, other cost effective hydrogen permeable materials such as Nb, V, and those alloys [13-14] can replace Pd. After Pd-plating, a thin-film of proton conductive electrolyte is deposited on the Pd layer and a thin-film of the cathode is deposited on the proton conductor layer.

2.2. Proton conductive material

Arrhenius plots of major proton conductors [8, 15] indicate that doped $BaZrO_3$ generally shows a higher ionic conductivity than $SrZrO_3$. However, the lattice parameter and the thermal expansion coefficient of barium oxides differ substantially from those of Pd. On the other hand, the lattice parameter and the thermal expansion coefficient of strontium-based perovskite oxides are relatively close to those of Pd used for the hydrogen permeable layer; the thermal expansion

coefficients of Pd, $SrZrO_3$, and $BaZrO_3$ are 11.8×10^{-6}/K, 9.87×10^{-6}/K, and 6.90×10^{-6}/K, respectively, while the lattice parameters of the *a*-axis at room temperature are 0.389 nm, 0.410 nm, and 0.419 nm, respectively [16]. We assume that the thermal expansion coefficient and the lattice parameter of an electrolyte are required to be close to those of th Pd layer to stabilize the interfacial structure between the electrolyte and Pd layers. Therefore, strontium zirconium oxide with yttrium doping for higher ionic conductivity, $Sr(Zr_{0.8}Y_{0.2})O_{3-\delta}$, was used as the proton conductive electrolyte material.

2.3. Cathode electrode material

Perovskite type oxides, $LnMO_3$ (Ln=La, Pr, Sm, M=Mn, Fe, Co, etc.), which consist of rare earth and 3d transition metals, have been used as cathode electrode materials in SOFC. The superior electron conductivity and oxygen ion conductivity are important for cathode materials to enhance power generation performance. In this study, $(La_{0.6}Sr_{0.4})(Co_{0.2}Fe_{0.8})O_{3-\delta}$ was used as the cathode material since it shows relatively good electron as well as superior ionic conductivities [17].

3. Experimental

3.1. Cell structure

(1) Preparation of the stainless steel porous support substrate consists of sintered alloy powders

SUS316L (Fe-17Cr-12Ni-2Mo mass%) spherical powders and stainless steel SUS430 (Fe-17Cr mass%) spherical powders were produced by nitrogen gas atomization. To prepare a sintered porous substrate with 1-mm height and 18-mm diameter, alloy SUS316L or SUS430 powders with 1–20-μm diameter were densely packed into an alumina crucible with a 1-mm height and a 18-mm diameter, and vacuum (1×10^{-5} Torr) sintered at 1050 °C for 90 min. To flatten the surface before Pd plating, a single side of the sintered porous substrate was rough polished followed

by mirror polishing.

(2) Pd plating on the surface of sintered porous substrates

A mask was used to cover the backside of the sintered porous substrate and only the other side was electroplated with Pd. Each specimen was initially immersed into a 10 mass% sodium hydroxide solution to remove impurities on its surface. Then it was immersed into a 10 mass% hydrochloric acid solution to remove the passive oxide films on the surface of the sintered powders. Next, Pd electroplating was conducted, using an alkali type solution at room temperature. Afterwards the specimen was washed with water followed by drying. The treatment time at a current density of 1.0 mA/dm^2 was adjusted to achieve a thickness between 5 and 15 μm. In the treatment, each specimen was placed as the cathode, and a Pt-coated titanium plate was used as the anode.

(3) Deposition of the electrolyte and cathode layers

$Sr(Zr_{0.8}Y_{0.2})O_{3-\delta}$ and $(La_{0.6}Sr_{0.4})(Co_{0.2}Fe_{0.8})O_{3-\delta}$ layers were deposited by PLD, using an excimer laser with a wavelength of 248 nm. To obtain satisfactory crystallinity and to realize the target values for the chemical compositions, deposition conditions were optimized. Target materials of $Sr(Zr_{0.8}Y_{0.2})O_{3-\delta}$ and $(La_{0.6}Sr_{0.4})(Co_{0.2}Fe_{0.8})O_{3-\delta}$ used in this study were prepared by spark plasma sintering. Primary deposition conditions for $Sr(Zr_{0.8}Y_{0.2})O_{3-\delta}$ were as follows: oxygen partial pressure of 50 mTorr, laser frequency of 8 Hz, laser-output density of 0.53 J/cm^2, and substrate temperature of 400 °C. $Sr(Zr_{0.8}Y_{0.2})O_{3-\delta}$ films with an area of 18-mm diameter were deposited on the Pd-plated side of the substrate with the same 18-mm diameter. On the other hand, primary deposition conditions for $(La_{0.6}Sr_{0.4})(Co_{0.2}Fe_{0.8})O_{3-\delta}$ were as follows: oxygen partial pressure of 50 mTorr, laser frequency of 4 Hz, laser-output density of 0.53 J/cm^2, and substrate temperature of 650 °C. $(La_{0.6}Sr_{0.4})(Co_{0.2}Fe_{0.8})O_{3-\delta}$ films with a 12-mm diameter deposition area were deposited

on $Sr(Zr_{0.8}Y_{0.2})O_{3-\delta}$ layers.

3.2. Characterization

(1) Crystal structure and microstructure characterization

For analyzing crystal structure of the deposited films, X-ray diffraction (XRD, Panalytical X' pert MRD) was used, and for investigating microstructures of the cell, field emission scanning electron microscopy (SEM, Hitachi S-4800 FE-SEM) and filed emission transmission electron microscopy (TEM, Hitachi HF-2000 FE-TEM) were used.

(2) Arrhenius plots for proton conductivity

Arrhenius plots for the proton conductivity of the cell were obtained from measuring alternating-current impedance in dry Ar and wet Ar with a 4194A (Agilent Technologies) impedance analyzer. Conditions of alternating-current impedance measurement were as follows: measurement frequency of 100 to 400 MHz, constant current of 20 mA, humidification temperature of 40 °C for wet Ar.

(3) Evaluation of the single-cell performance

The single-cell performances, current density - cell voltage and current density - power density curves, were measured by an evaluation system, TOYO-Auto PEM (TOYO Corporation) utilizing TOYO TFT integrated software. Both sides of the sample cell were connected to a TOYO-Auto PEM system by Pt paste and Pt wire. The power generation properties were evaluated under the following test conditions: cell temperature at 400 °C and 450 °C, cathode humidification temperature of 25 °C, anode humidification temperature of 25 °C, hydrogen feed rate of 0.15 L/min, and air feed rate of 0.10 L/min.

4. Results and discussion

4.1. Effects of thermal expansion coefficients of metallic support substrates on structural stability

First, the effects of thermal expansion coefficient differences of metallic supports on structural stability were investigated. In this test, Pd-plated porous-substrates that employed different alloy grades with different thermal expansion coefficients, SUS316L (18.5×10^{-6}/K) and SUS430 (11.9×10^{-6}/K), were used. Prepared samples were heated at 700 °C for 20 min in an Ar atmosphere.

Figure 2 shows the SEM image of the surface for each sample after heating. Several cracks are observed in the Pd layer for the sample using SUS316L powders, whereas cracks are hardly observed for the sample using ferritic SUS430 powders. Those observed cracks are attributed to the difference in the thermal expansion coefficients between SUS316L (18.5×10^{-6}/K) powders and Pd (11.8×10^{-6}/K) layer, that is to say, tensile stresses are generated in the thin Pd-layer during heating because the expansion of the substrates consists of SUS316L powders is larger than that of Pd layer. On the other hand, the thermal expansion coefficient of the SUS430 powder (11.9×10^{-6}/K) is extremely close to Pd (11.8×10^{-6}/K) and it likely prevented crack initiations. It must be noted here that Herbert *et al.* [18] reported that for a given chemical composition, the thermal expansion coefficient of a porous body composed of sintered metallic powders has the same value as that of the dense bulk sample. Those observed cracks may breach sealing properties, which leads to mixing of hydrogen and oxygen and degrades cell performance. Consequently, sample cells were prepared using ferritic SUS430 powders in the following sections.

4.2. Microstructure and crystal structure of the cell

Figure 3 shows the cross-sectional TEM image of the cell. An approximately 1.2-μm thick layer of $Sr(Zr_{0.8}Y_{0.2})O_{3-\delta}$ is precisely and uniformly deposited on a Pd-plated porous substrate consists of sintered SUS430 powders. In addition, an approximately 100-nm thick layer of

$(La_{0.6}Sr_{0.4})(Co_{0.2}Fe_{0.8})O_{3-\delta}$ is deposited on the $Sr(Zr_{0.8}Y_{0.2})O_{3-\delta}$ layer.

Figure 4 shows the XRD patterns of the cell before and after the depositions of the $Sr(Zr_{0.8}Y_{0.2})O_{3-\delta}$ and $(La_{0.6}Sr_{0.4})(Co_{0.2}Fe_{0.8})O_{3-\delta}$ layers. Only a single phase, which is assigned to $Sr(Zr_{0.8}Y_{0.2})O_{3-\delta}$, is observed. This observation differs from the sintered body used as the target because the target exhibits a second phase of SrY_2O_4. This difference is considered to be due to non-equilibrium conditions in the deposited film. The XRD patterns corresponding to $(La_{0.6}Sr_{0.4})(Co_{0.2}Fe_{0.8})O_{3-\delta}$ are not observed in Fig.4, and this is probably due to the extreme thin film, approximately 100-nm thick, as shown in Fig. 3. Although the depositions of $Sr(Zr_{0.8}Y_{0.2})O_{3-\delta}$ and $(La_{0.6}Sr_{0.4})(Co_{0.2}Fe_{0.8})O_{3-\delta}$ were conducted at elevated temperatures of 400 °C and 650 °C, respectively, no noticeable cracks are detected on the deposited layers by SEM observation. It is attributed to similar thermal expansion coefficients among $Sr(Zr_{0.8}Y_{0.2})O_{3-\delta}$ (9.87×10^{-6}/K) layer, Pd (11.8×10^{-6}/K) layer, and sintered SUS430 (11.9×10^{-6}/K) powders.

4.3. Proton conductivity of the prepared $Sr(Zr_{0.8}Y_{0.2})O_{3-\delta}$ film at low temperatures

The conductivity of proton conductors is generally enhanced due to existing hydrogen and/or H_2O in the atmosphere, which indicates lower activation energy compared to that in the atmosphere without hydrogen and/or H_2O. Figure 5 shows the Arrhenius plots of $Sr(Zr_{0.8}Y_{0.2})O_{3-\delta}$ films prepared on the Pd-coated stainless steel substrate in dry and wet Ar at low temperatures of approximate 200 to 400 °C , which are calculated by results of alternating-current impedance measurement of the cell. The obtained activation energy of $Sr(Zr_{0.8}Y_{0.2})O_{3-\delta}$ in wet Ar is 0.51 eV, and it is smaller than 0.61 eV in dry Ar. These obtained values in dry and wet Ar are almost equivalent to the reported activation energies of $Ba(Zr_{0.7}Pr_{0.1}Y_{0.2})O_{3-\delta}$, one of the major proton conductors, with 0.51 eV in wet Ar and 0.65 eV in dry Ar [19]. Therefore, it is considered that the main carrier of $Sr(Zr_{0.8}Y_{0.2})O_{3-\delta}$ prepared by PLD in this study at low temperatures is hydrogen. In addition, the measured ionic conductivities are equivalent to values in previous report of

$Sr(Zr_{0.8}Y_{0.2})O_{3-\delta}$ prepared by sputtering [20].

4.4. Demonstration of the cell performance

To demonstrate the cell performance at low temperatures, the power generation properties of the prepared cell, using sintered ferritic SUS430 powders with thin hydrogen permeable Pd-plating, 1.2-μm thick layer of proton conductive $Sr(Zr_{0.8}Y_{0.2})O_{3-\delta}$ as an electrolyte, and an approximately 100-nm thick layer of $(La_{0.6}Sr_{0.4})(Co_{0.2}Fe_{0.8})O_{3-\delta}$ as a cathode, were investigated at the cell temperatures of 400 °C and 450 °C. These temperatures are much lower than the conventional operating temperatures of SOFC, i.e. from 700 °C to 1000 °C. Figure 6 shows the current density – cell voltage and current density - power density curves. The power generation performance of the proposed cell in this study was demonstrated for the first time at low temperatures of 400 °C and 450 °C, while obtained maximum power densities are 1.2 mW/cm^2 and 2.2 mW/cm^2 respectively, 2 - 3 orders of magnitude lower than typically reported perforamnce levels and required output levels in a commercial device. Obtained open circuit voltages (OCV), 0.63 V at 400 °C and 0.67 V at 450 °C, are lower than the normally reported OCV value of approximate 1 V, therefore, there might be some leakage through the cell due to defects in Pd-plated layers, which can reduce power output densities. Although, lower rate of Pd-plating and increasing the thickness of Pd-layers are considered to be effective to improve sealing properties of the cells, those approaches will increase cell costs. Instead, using smaller alloy powders and employing higher sintering temperature are assumed to be effective, which can decrease each pore size in the porous bodies composed of sintered alloy powders and those smaller pores are tend to be filled in densely under the coating of hydrogen permeable layers. One of the additional key factors to improve cell performance is considered to enhance proton conductivity of the electrolyte, because obtained proton conductivity in this study as shown in fig.5 is still 1-2 digit lower than that of the reported value for other proton conductive materials like $Ba(Zr_{0.8}Y_{0.2})O_3$ [21]. Another key factor

for the improvement is considered to increase reaction interfaces in the cathode side. E. Fabbri, D. Pergolesi, and E. Traversa have reported [22] the necessity of the porous structure for the cathode, especially for SOFCs using proton conductive electrolytes because water must be able to evaporate unless the cathode material also exhibits proton conductivity. Moreover, according to their report, a cathode structure comprised of both a proton conductor phase and an O_2/e^- conductor can efficiently increase the reaction interfaces. In this study, a dense film is used for the cathode without a porous structure, which might reduce reaction interfaces and lowered cell performance.

In our future research, improvements of cell performance will be studied, focusing on those key factors including the increase of reaction interfaces, important for the improvement of the cell performance, and replacing expensive Pd-layer by other cost effective hydrogen permeable materials like V, Nb, and those alloys [13-14].

4. Conclusions

The present results can be summarized as follows:

1) A novel cell structure for proton conductive type low-temperature SOFC with metallic support was proposed, using porous stainless steel support substrates combined with thin hydrogen permeable layers, thin-film electrolyte of proton conductor, and thin-film cathode layer, in which the metallic support consists of sintered ferritic stainless steel powders whose thermal expansion coefficient is close to hydrogen permeable layers and proton conductive electrolytes.

2) In preparing the test cell, an approximately 1.2-μm thick proton conductive layer of $Sr(Zr_{0.8}Y_{0.2})O_{3-\delta}$, was successfully uniformly deposited by PLD on Pd-plated sintered porous substrates consists of ferittic SUS430 powders. A 100-nm thick cathode layer of $(La_{0.6}Sr_{0.4})(Co_{0.2}Fe_{0.8})O_{3-\delta}$ was deposited on $Sr(Zr_{0.8}Y_{0.2})O_{3-\delta}$ layer uniformly by PLD.

3) According to obtained Arrhenius plots, hydrogen is considered to be the main carrier at low temperatures of 400 °C for $Sr(Zr_{0.8}Y_{0.2})O_{3-\delta}$ prepared by PLD in this study.

4) The power generation performance at a low temperature of 400 °C was demonstrated for the first time, while obtained power density is still low, 1.2 mW/cm^2.

Acknowledgements

H. Funakubo and K. Uchiyama would like to thank to the Adaptable and Seamless Technology Transfer Program through target-driven R&D, JST and the Advanced Low Carbon Technology Research and Development Program, JST for their financial support.

References

[1] A. B. Stambouli, E. Traversa, Renewable and Sustainable Energ. Rev., 6 (2002) 433.

[2] E. D. Wachsman, S. C. Singhal, Electrochem. Soc. Interf., Fall (2009) 38.

[3] N. Laosiripojana, W. Wiyaratn, W. Kiatkittipong, A. Arpornwichanop, A. Soottitantawat, and S. Assabumrungrat, Eng. J., 13 (2009) 65.

[4] C. R. He, W.G. Wang, Fuel Cells, 5 (2009) 630

[5] H. Iwahara, T. Yajima, T. Hibino, and H. Ushida, J. Electrochem. Soc., 140 (1993) 1687.

[6] T. Shimada, C. Wen, N. Taniguchi, J. Otomo, and H Takahashi, J. Power Sour., 131 (2004) 289.

[7] H. Iwahara, T. Esaka, H. Uchida, and N. Maeda, Solid State Ionics, 3-4 (1980) 359.

[8] K. D. Kreuer, Solid State Ionics, 97 (1997) 1

[9] N. Ito, M. Iijima, K. Kimura, S. Iguchi, J. Power Sour., 152 (2005) 200.

[10] S. Shin, H. Huang, M. Ishigame, and H. Iwahara, Solid State Ionics, 47 (1990) 910.

[11] T. Higuchi, T. Tsukamoto, S. Yamaguchi, N. Sata, K. Hiramoto, M. Ishigame, and S. Shin, Jpn. J. Appl. Phys., 41 (2002) 6440.

[12] K. Yamakawa, M. Ege, B. Ludescher, M. Hirscher, H. Kronmuller, J. Alloys and Compounds, 17-23 (2001) 321.

[13] T. Nambu, K. Shimizu, Y. Matsumoto, R. Rong, N. Watanabe, H. Yukawa, M. Morinaga, I. Yasuda, J. Alloys and Compounds, 588-592 (2007) 446-447.

[14] H. Yukawa, T. Nambu, Y. Matsumoto, J. Alloys and Compounds, S881-S884 (2011) 509S

[15] K. D. Kreuer, Chem. Mater., 8 (1996) 610.

[16] Y. Zhao, D. J. Weidner, Phys. Chem. Mine., 18 (1991) 294.

[17] E. V. Tsipis, V.V. Kharton, Solid State Electrochem., 12 (2008) 1039.

[18] D. Herbert, G. Christian, Adv. Powder. Metall. Part. Mater., 2 (2010) 10.1

[19] E. Fabbri, Lei Bi, H. Tanaka, D. Pergolesi, E. Traversa, Adv. Funct. Mater., 21 (2011) 158.

[20] M. Arab Pour Yazdi, P.Briois, S. Georges, A. Billard, Solid State Ionics, 180 (2009) 1246.

[21] P. Plonczak, et al, Adv. Funct. Mater, 21 (2011) 2764

[22] E. Fabbri, D. Pergolesi and E. Traversa, Sci. Tech. Adv. Mater., 11 (2010) 044301.

Figure Captions

Fig. 1. Schematic illustration of the proposed cell structure for low-temperature solid oxide fuel cell, SOFC.

Fig. 2. SEM images after heating to 700 °C in an Ar atmosphere of (a) top surface and (b) cross-section of Pd-plated sintered SUS316L powder, and (c) top surface and (d) cross-section of Pd-plated sintered SUS430 powder.

Fig. 3. Cross-sectional TEM image of $Sr(Zr_{0.8}Y_{0.2})O_{3-\delta}$ and $(La_{0.6}Sr_{0.4})(Co_{0.2}Fe_{0.8})O_{3-\delta}$ layers deposited on plated Pd.

Fig. 4. XRD profiles of (a) after and (b) before depositions of the $Sr(Zr_{0.8}Y_{0.2})O_{3-\delta}$ and $(La_{0.6}Sr_{0.4})(Co_{0.2}Fe_{0.8})O_{3-\delta}$ layers.

Fig. 5. Arrhenius plots of the conductivity for $Sr(Zr_{0.8}Y_{0.2})\ O_{3-\delta}$ electrolyte deposited by PLD.

Fig. 6. Current density - cell voltage and current density - power density curves of the prepared cell measured at 400 °C and 450 °C.

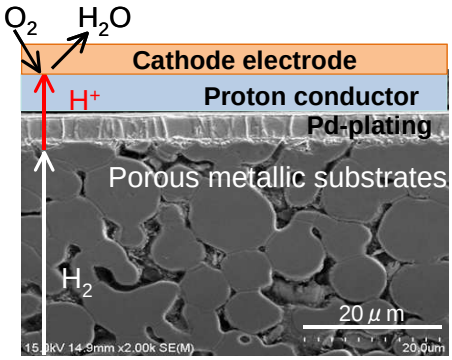

Fig. 1. Schematic illustration of the proposed cell structure for low-temperature solid oxide fuel cell, SOFC.

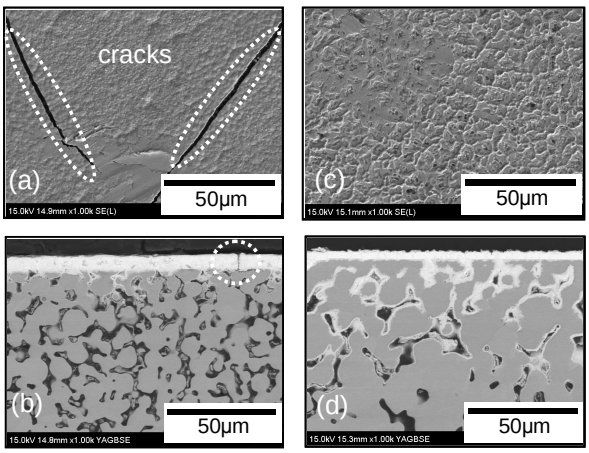

Fig. 2. SEM images after heating to 700°C in an Ar atmosphere of (a) top surface and (b) cross-section of Pd-plated sintered SUS316L powder, and (c) top surface and (d) cross-section of Pd-plated sintered SUS430 powder.

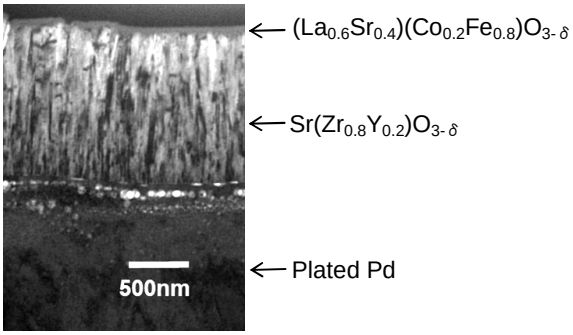

Fig. 3. Cross-sectional TEM image of $Sr(Zr_{0.8}Y_{0.2})O_{3-\delta}$ and $(La_{0.6}Sr_{0.4})(Co_{0.2}Fe_{0.8})O_{3-\delta}$ layers deposited on plated Pd.

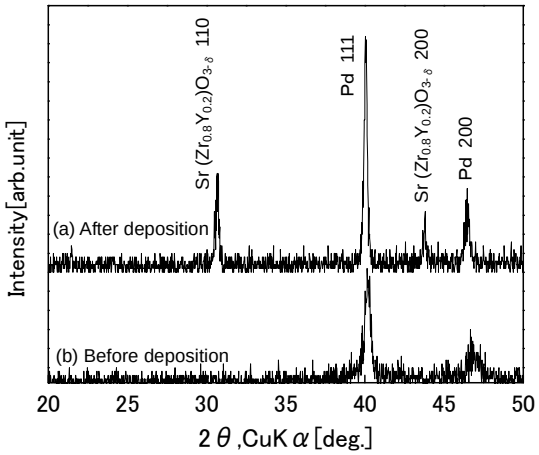

Fig. 4. XRD profiles of (a) after and (b) before depositions of the $Sr(Zr_{0.8}Y_{0.2})O_{3-\delta}$ and $(La_{0.6}Sr_{0.4})(Co_{0.2}Fe_{0.8})O_{3-\delta}$ layers.

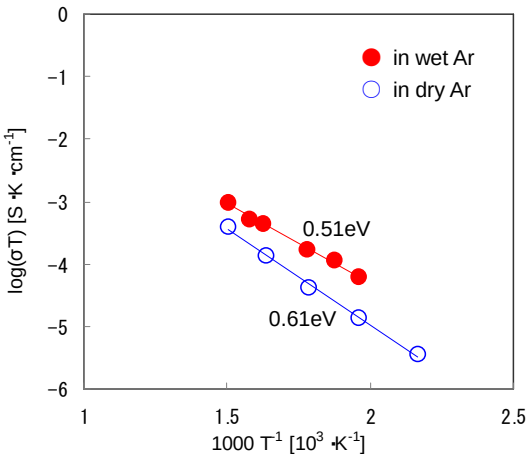

Fig. 5. Arrhenius plots of the conductivity for $Sr(Zr_{0.8}Y_{0.2})O_{3-\delta}$ electrolyte deposited by PLD.

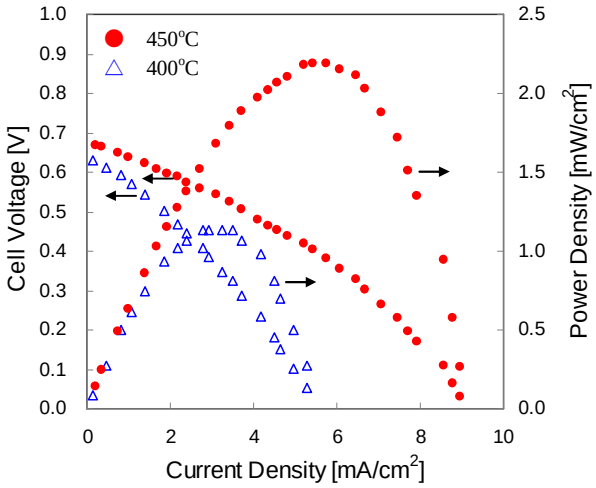

Fig. 6. Current density – cell voltage and current density – power density curves of the prepared cell measured at 400°C and 450°C.

Highlights

A novel cell structure using metallic support for low-temperature SOFC was proposed.

Ferritic porous metal support was combined with thin film of proton conductor SZYO.

Cell performance at 400°C of the proposed cell was demonstrated for the first time.